Spin interactions in an Anderson-Hubbard model

1998 J. Phys.: Condens. Matter 10 639

(http://iopscience.iop.org/0953-8984/10/3/015)

J. Phys.: Condens. Matter **10** (1998) 639–655. Printed in the UK PII: S0953-8984(98)87520-6

Spin interactions in an Anderson–Hubbard model

Yolande H Szczech, Michael A Tusch and David E Logan

Physical and Theoretical Chemistry Laboratory, Oxford University, South Parks Road, Oxford OX1 3QZ, UK

Received 11 September 1997

Abstract. We study the magnetic properties of a site-disordered Anderson–Hubbard model at half-filling on a simple cubic lattice, via a mapping of its low-frequency transverse spin excitations onto those of an effective underlying Heisenberg model with self-consistently determined exchange couplings. Exact in the strong-coupling limit, the mapping remains accurate over the dominant region of the phase plane where the ground state is a disordered antiferromagnet. The effect of disorder and interaction strength on the resultant exchange couplings is examined in detail, and rationalized microscopically. Frustration is found to occur, even within the antiferromagnetic phase, although the ground state is shown to be stable with respect to zero-point quantum spin fluctuations. To probe finite-temperature magnetic properties, an Onsager reaction-field approach to the effective Heisenberg model in the paramagnetic phase is employed. We focus on the effect of disorder on the Néel temperature and the nature of the thermal transition to the ordered phase.

1. Introduction

One of the most challenging problems in the study of disordered, interacting electron systems is that of local moment formation and subsequent interaction. Anderson–Hubbard models (AHM) are notionally the simplest with which to investigate such matters, wherein the many complexities of strongly interacting electrons—captured at the level of the pure Hubbard model—are compounded by the presence of disorder, leading to local moment formation on a strongly inhomogeneous scale and a rich variety of potential magnetic and electric phases.

In this paper, we consider the magnetic properties of a site-disordered AHM at half-filling on a $d = 3$ simple cubic lattice, focusing in particular on disordered antiferromagnetic (AF) phases of the model. The approach taken derives from a technique recently developed [1, 2] and applied to the ubiquitous AF phase of the corresponding pure Hubbard model, the low-energy transverse spin excitations of which are mapped approximately onto those of an effective Heisenberg model; the exchange couplings of the latter being determined self-consistently, dependent on the on-site interaction U and not *a priori* constrained to nearest-neighbour (NN) interactions. The mapping becomes exact in the strong-coupling limit $U/t \to \infty$ (with t the hopping amplitude), where the Hubbard model maps rigorously onto a spin-1/2 AF Heisenberg model with purely NN couplings $J_\infty = 4t^2/U$. More significantly, for all but very low interaction strengths ($U/t \gtrsim 2-3$), linear spin-wave theory applied to the effective Heisenberg model is found [1, 3] to reproduce quantitatively the low-energy spectral density of transverse spin excitations obtained for the pure Hubbard model via a random-phase approximation (RPA) about the broken-symmetry (Néel) unrestricted Hartree–Fock (UHF) ground state. And the latter approach—UHF + RPA—has been shown by several groups [4, 5] to account well for the physics of the $d \geqslant 2$ half-filled Hubbard

0953-8984/98/030639+17$19.50

model on bipartite lattices at $T = 0$ (despite the incorrect, but not uncommonly asserted, view that such an approach is intrinsically a weak-coupling one).

A distinct advantage of the effective spin Hamiltonian is that it suggests a potentially straightforward route to thermodynamic properties of the Hubbard model in a temperature regime dominated by the low-energy spin-wave-like excitations—one that in practice extends well above the Néel temperature. For the thermal paramagnetic phase of the pure Hubbard model, this has been considered [1, 2] via a simple Onsager reaction-field (ORF) approach. The latter provides in effect a self-consistent modification of conventional molecular-field theory to account for the effects of local spin correlations, that are crucial not only in quantitative terms but also in obtaining agreement with e.g. the dimensional dictates of the Mermin–Wagner theorem. For the $d = 3$ Hubbard model, the approach has been shown [1, 2] to yield very good agreement with quantum Monte Carlo results for Néel temperatures, magnetic susceptibilities and spin correlations over a wide range of temperatures and interaction strengths; and, as discussed in reference [1], it appears to transcend successfully the inherent limitations of a wide variety of previous approaches to finite-temperature magnetism in the Hubbard model (see e.g. reference [6]).

The above strategy—both the mapping and the ORF approach—are generalizable to magnetically ordered phases of the disordered AHM (where the mapping is again exact for strong coupling [7]). This we consider here, drawing in particular on previous results for both the $T = 0$ phase diagram of the AHM with Gaussian site disorder, obtained at the mean-field level of broken-symmetry UHF [8]; and on the full collective excitation spectrum about the inhomogeneous ground states [3] obtained via the RPA.

The theoretical approach, and the validity of the underlying mapping, are sketched in section 2. In contrast to much conventional work on localized-spin magnetism, where the distribution of exchange couplings is specified *a priori*, the probability densities of effective exchange couplings in the present problem stem from the underlying system of interacting, itinerant electrons. These are considered and rationalized in section 3, together with a discussion of the extent to which frustration is induced in the exchange coupling distributions. The stability of the disordered AF phase with respect to zero-point quantum spin fluctuations is then considered at one-loop level, and a microscopic rationale for the stability of the phase suggested. Finite-temperature properties in the thermal paramagnetic phase are considered in section 4. The ORF approach in the presence of disorder, and its connection to other approaches, is first discussed. The effect of disorder on the Néel temperature of the AHM is then considered, together with the predicted characteristics of incipient magnetic ordering at the thermal phase boundary.

2. Theoretical approach

The Hamiltonian we consider is the site-disordered Anderson–Hubbard model (AHM):

$$H = \sum_{i,\sigma} \epsilon_i n_{i\sigma} - t \sum_{\langle ij\rangle,\sigma} c^{\dagger}_{i\sigma} c_{j\sigma} + \tfrac{1}{2} U \sum_{i,\sigma} n_{i\sigma} n_{i-\sigma} \tag{1}$$

where t is the nearest-neighbour (NN) hopping matrix element, U is the on-site Coulomb interaction and the $\langle ij\rangle$ sum is over nearest-neighbour sites on a $d = 3$ simple cubic lattice. The site energies $\{\epsilon_i\}$ are drawn randomly from a common Gaussian distribution $g(\epsilon)$ of variance Δ^2, and we focus on half-filling. We here study the problem numerically, with systems of $N = 216$ sites, sampling a sufficient number of disorder realizations to gain good statistics.

An analysis of the $T = 0$ phase diagram of this model at UHF level is given in reference [8]. All ground states are found to be Ising-like, with local moments lying along a common z-axis, and with $\langle S_z^{\rm tot}\rangle_{\rm HF} = 0$. The dominant magnetic phase in the $(\Delta/t, U/t)$ plane is the disordered AF. Here, the magnitudes of the local moments $\mu_i = 2\langle S_{iz}\rangle_{\rm HF}$ are disordered, but their phases are locked in AF alignment, such that the magnetic structure factor $\mu(\boldsymbol{q}) = N^{-1}|\sum_i \mu_i e^{i\boldsymbol{q}\cdot\boldsymbol{r}_i}|$ shows a strong peak at $\boldsymbol{q} = \boldsymbol{\pi}$, with little weight at other $\boldsymbol{q}$-vectors. At low $U/t \sim 2$–3 a transition [9] occurs to a SG phase, for which $\mu(\boldsymbol{q})$ exhibits peaks $O(N^{-1})$ at many $\boldsymbol{q}$-vectors. A non-magnetic phase occurs at still smaller interaction and disorder strengths, with $\mu_i = 0$ for all sites. Metallic (M) and insulating (I) phases are also found, with the dominant MIT being M $\rightarrow$ gapless I, driven by Anderson localization of quasiparticle states at the Fermi level.

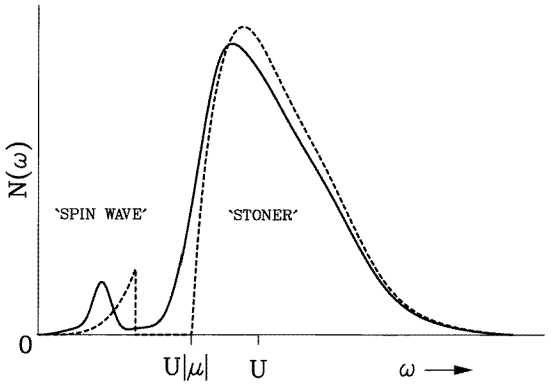

Figure 1. Schematic density of RPA transverse excitations in the non-disordered limit (dashed line) and in the presence of significant disorder (solid line).

For both the pure ($\Delta = 0$) Hubbard model [1, 4, 5] and the AHM [3], collective particle–hole excitations about the underlying broken-symmetry mean-field ground states follow via a random-phase approximation (RPA). For the Ising-like UHF ground states, the RPA Hamiltonian block diagonalizes into two sectors [1, 9]: a transverse spin channel corresponding to spin fluctuations away from the local moment axis, and a mixed longitudinal spin and charge channel comprising excitations along this axis. The lowest-energy collective excitations occur in the transverse spin channel, and include the zero-frequency Goldstone modes describing a global spin rotation. For the pure Hubbard model, as illustrated schematically in figure 1, the resultant transverse spin spectrum consists [1, 3] of a prominent low-frequency band extending down to zero frequency, together with a high-energy band of weakly renormalized Stoner-like excitations, to which there is a gap of the order of the single-particle band gap of magnitude $U|\mu|$ (where $|\mu_i| = |\mu|\ \forall i$). To a very good approximation, the low-energy transverse spin excitations are found to be spin waves for all but very low U/t. Because of the gap to Stoner processes, thermodynamic properties of the model are naturally governed by the spin-wave-like excitations up to temperatures well in excess of the Néel temperature $T_{\rm N}$, for all but the weakest interaction strengths.

In references [1, 2] it was shown that an effective underlying spin Hamiltonian which accurately describes the low-energy excitations may be obtained by comparison of the linear spin-wave equations of an arbitrary Heisenberg model with the site-resolved RPA equations for the Hubbard model. The resultant Hamiltonian is given by

$$H_{\rm Heis} = \tfrac{1}{2}\sum_{\substack{i,j\\(j\neq i)}} J_{ij}\boldsymbol{S}_i\cdot\boldsymbol{S}_j \qquad (2)$$

with $\boldsymbol{S}$ a spin-$\frac{1}{2}$ operator, and where the effective exchange couplings—which are not confined to nearest neighbours—are given explicitly in terms of the static RPA transverse susceptibility $\boldsymbol{\chi}(0)$ by

$$J_{ij} = 2|\mu_i \mu_j|[\boldsymbol{\chi}^{-1}(0)]_{ij} \qquad j \neq i. \tag{3}$$

The full frequency-dependent susceptibility matrix $\boldsymbol{\chi}$ is in turn given by

$$\boldsymbol{\chi}(\omega) = {}^0\boldsymbol{\chi}(\omega)[\mathbf{I} - U\,{}^0\boldsymbol{\chi}(\omega)]^{-1} \tag{4}$$

where ${}^0\boldsymbol{\chi}$ is the UHF transverse susceptibility

$${}^0\chi_{ij}(\omega) = \mathrm{i}\int \mathrm{d}t\ \mathrm{e}^{\mathrm{i}\omega t}\langle 0|\mathcal{T}\{S_i^-(t)S_j^+\}|0\rangle_{\mathrm{HF}} \tag{5}$$

with $|0\rangle_{\mathrm{HF}}$ the self-consistent UHF ground state. The mapping becomes exact as $U/t \to \infty$, where $J_{ij} = 4t^2/U$ for i, j nearest neighbours (NN) and zero otherwise; and for the pure Hubbard model is found to be quantitatively accurate down to $U/t \simeq 2$–3. At all interaction strengths, it preserves precisely the RPA zero-frequency transverse susceptibilities $\{\chi_{ij}(0)\}$.

We now consider the validity of the above mapping for the AHM. As discussed in reference [1], the mapping is accurate provided that there is a persistent separation between the low-energy spin-wave-like excitations and the higher-energy Stoner-like processes; i.e. provided in practice that a discernible low-frequency band is present in the full RPA spectrum, comprising transverse excitations with a significant degree of spin-wave-like character.

The latter has been considered in detail in reference [3], and the typical effect of disorder on the collective transverse spin spectrum is schematized in figure 1 (see also e.g. figure 5 of reference [3]). The gap between the spin-wave-like and Stoner-like bands becomes a pseudogap, and the low-energy spin-wave-like band is softened with disorder; these effects naturally becoming more pronounced with increasing disorder or diminishing interaction strength. Nonetheless, as anticipated in reference [3] and confirmed by direct comparison of the full RPA transverse spin spectrum with that arising from the effective H_{Heis}, equation (2), the mapping remains accurate throughout the major portion of the disordered AF phase in the (Δ, U) plane, breaking down only on approaching the AF–SG border (occurring at low $U/t \sim 2$–3). It is therefore on the disordered AF phase of the AHM that we focus in the present work.

3. Effective exchange couplings

For the pure Hubbard model [1, 2], the dominant exchange couplings for all U/t are nearest neighbour (NN); next-nearest (2NN) and third-nearest-neighbour (3NN) couplings are an order of magnitude smaller (although they have a significant effect on e.g. T_{N} for $U/t \lesssim 15$ [2]). For all interaction strengths the effective exchange couplings reinforce the underlying antiferromagnetic structure of the mean-field ground state, i.e. they are positive (antiferromagnetic) between sites on different sublattices and negative (ferromagnetic) between sites on the same sublattice. As U/t is lowered, NN exchange couplings are diminished from their asymptotic form $J_{\mathrm{NN}} = 4t^2/U$ (which in practice is reached by $U/t \sim 20$), reaching a maximum at $U/t \simeq 10$ and decreasing steadily to zero thereafter (see figure 5 below).

On the introduction of disorder, the dominant exchange couplings remain NN. Figure 2 shows the probability distribution, $P_{\mathrm{NN}}(J)$, of NN exchange couplings for fixed $U/t = 12$ and a range of values of Δ/t from 3 to 7.5. At the lowest value of Δ/t (figure 2(a)), a

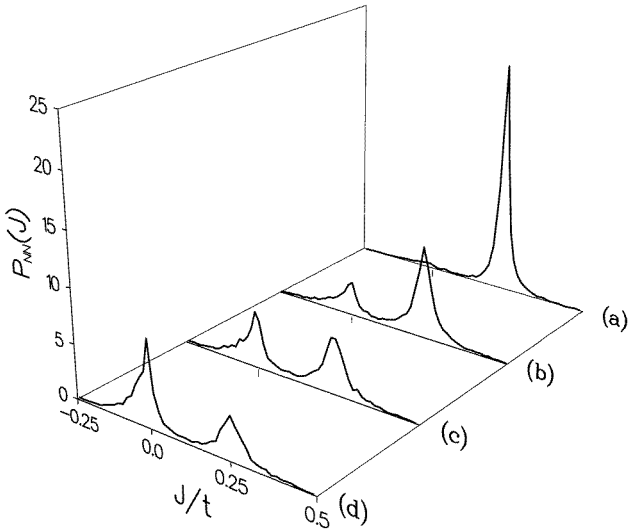

Figure 2. Probability distribution of nearest-neighbour exchange couplings $P_{\mathrm{NN}}(J)$ for fixed interaction strength $U/t = 12$ and $\Delta/t = 3$ (a), 4.5 (b), 6 (c) and 7.5 (d).

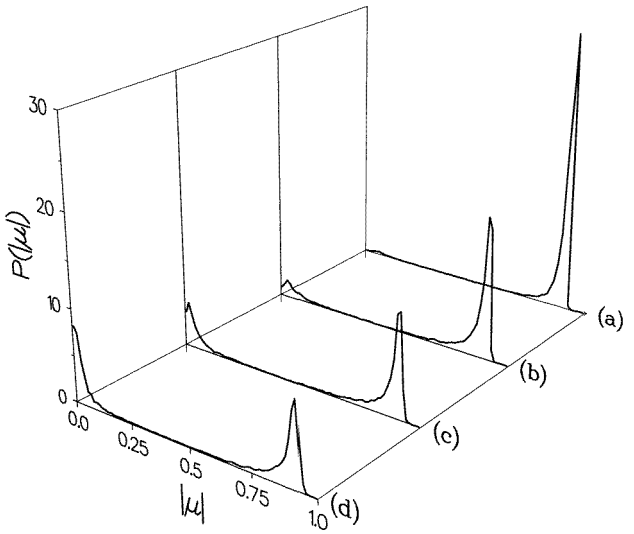

Figure 3. Probability distribution of local moment magnitudes $P(|\mu|)$ for fixed $U/t = 12$ and $\Delta = 3$ (a), 4.5 (b), 6 (c) and 7.5 (d).

single sharp peak is evident, the maximum of which occurs very close to the corresponding $\Delta/t = 0$ value, $J^0_{\mathrm{NN}}/t = 0.241$. Increasing Δ/t to 4.5 causes the main peak to erode, together with the formation of a secondary peak centred on $J/t \sim 0$. For $\Delta/t = 6$, the two peaks are of comparable weight, while by $\Delta/t = 7.5$ the secondary peak is clearly dominant.

This bimodal behaviour of $P_{\mathrm{NN}}(J)$ may be rationalized, using equation (3), in terms of the probability distribution of local moment magnitudes $P(|\mu|)$. This is shown in figure 3

for the same $(\Delta/t, U/t)$ values as in figure 2. As discussed in reference [8], strong local moments exist on sites with bare site energies in the range $|\epsilon| \lesssim U/2$, while sites outside this range carry only weak moments. For $\Delta/t = 3$ (figure 3(a)), virtually all sites carry strong local moments, eroded only slightly from their $\Delta/t = 0$ values: hence the dominance of the single peak centred at $\sim J^0_{\rm NN}$. Increasing disorder (for given U/t) reduces the fraction of sites in the strong-moment range, with a concomitant increase in the number of relatively weak moments (figures 3(b)–3(d)). Couplings between these weak moments account for the secondary peak in $P_{\rm NN}(J)$, whose relative growth with increasing Δ/t naturally reflects the increasing proportion of such sites.

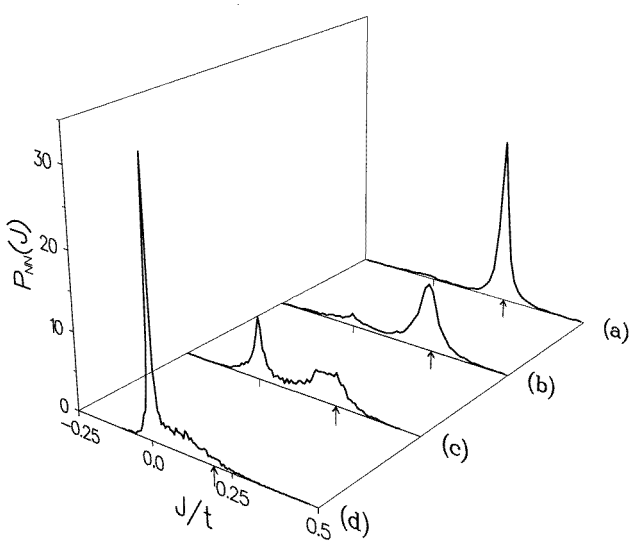

Figure 4. Probability distribution of NN exchange couplings $P_{\rm NN}(J)$ for fixed disorder strength $\Delta/t = 3$ and $U/t = 12$ (a), 9 (b), 6 (c) and 4.5 (d). For $\Delta = 0$, $P_{\rm NN}(J) = \delta(J - J^0_{\rm NN})$, indicated by an arrow.

A similar picture arises on fixing $\Delta/t = 3$ and lowering U/t towards the AF–SG border, as shown in figure 4. Here, the erosion of the 'AF' peak at positive J is more pronounced, since decreasing U/t shifts its position towards zero, such that by $U/t = 4.5$ (figure 4(d)) it appears merely as a shoulder on the main peak at $J/t = 0$. However, though most exchange couplings are here very weak, NN couplings do still act to reinforce the underlying antiferromagnetic structure, as can be seen in figure 5. This shows $\langle J_{\rm NN}\rangle$, where $\langle\cdots\rangle$ denotes an average over all NN exchange couplings and disorder realizations, as a function of interaction strength for fixed disorder $\Delta/t = 3$; together with the $\Delta = 0$ limit, $J^0_{\rm NN}(U)$, for comparison (which has been discussed in detail in reference [2]). As U/t is lowered from deep inside the AFI phase, both the disordered and non-disordered systems show the same trend: an initial increase, followed by a steady decrease. In the pure Hubbard model ($\Delta = 0$), for which the mean-field ground state has AFLRO for all U/t, $J^0_{\rm NN}(U)$ naturally remains finite down to the weakest interaction strengths [1, 2]. In the presence of disorder, by contrast, the occurrence of the SG phase at low interaction strengths suggests that $\langle J_{\rm NN}\rangle$ vanishes at finite U/t. While numerically difficult to obtain accurately, simple extrapolation of the $\Delta/t = 3$ curve of figure 5 to $\langle J_{\rm NN}\rangle = 0$ leads to $U_c/t \simeq 3.5$, which is indeed close to the phase boundary between the mean-field AF and SG phases

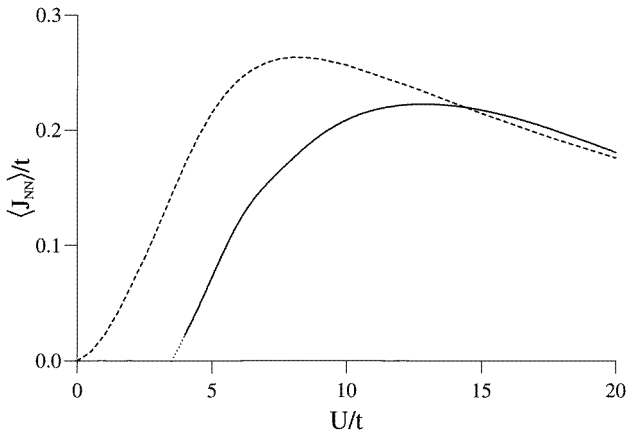

Figure 5. Average nearest-neighbour exchange coupling $\langle J_{\rm NN}\rangle$ as a function of interaction strength U/t for $\Delta/t = 3$ (solid line) and $\Delta/t = 0$ (dashed line). The Δ/t curve has been extrapolated to the AF–SG border (dotted line), as discussed in the text.

[8, 9]. Notice also from figure 5 that, for sufficiently large interaction strengths, addition of disorder enhances somewhat the average NN exchange coupling, an effect observed by Ulmke *et al* [10] in their QMC study of the infinite-dimensional AHM. Finally, we add that similar bimodal probability densities are found for 2NN and 3NN couplings, although (as for the pure Hubbard model [1, 2]) these are typically an order of magnitude smaller than the $J_{\rm NN}$.

Table 1. Percentage frustration in exchange couplings for $\Delta/t = 3$.

U/t	NN	2NN	3NN
12	1.48	5.01	6.33
9	5.19	15.59	14.03
6	13.36	31.43	25.27
4.5	23.68	41.43	33.58

We now consider the extent to which site-diagonal disorder introduces frustration into the effective exchange couplings. As discussed above, the effective exchange couplings of the pure Hubbard model exhibit no frustration whatever, reinforcing the underlying AFLRO of the mean-field ground state at all levels. For the disordered AHM, we find that the underlying magnetic ordering is again reinforced, but only on the average: frustration occurs, even within the AF phase. The degree of frustration is however much less extensive than might at first sight be suggested by the $P_{\rm NN}(J)$ distributions of figures 2 and 4 (reflecting the fact that the $\{J_{ij}\}$, given individually by equation (3), are not themselves independent random variables but are rather strongly correlated). To demonstrate this, we define a bond energy $F_{ij} = J_{ij}\mu_i\mu_j$ which, if negative, corresponds to a satisfied bond but, if positive, corresponds to a frustrated bond. Figure 6 shows $P_{\rm NN}(J)$ for all bonds (dark shading), and for frustrated NN bonds with $F_{ij} > 0$ (light shading), for $(\Delta/t, U/t) = (3, 6)$. The frustrated bonds are confined solely to the vicinity of the peak at $J/t \sim 0$, which corresponds to weak couplings between small moments. The large moments, which are strongly coupled, by contrast exhibit no frustration at all, and form the antiferromagnetic

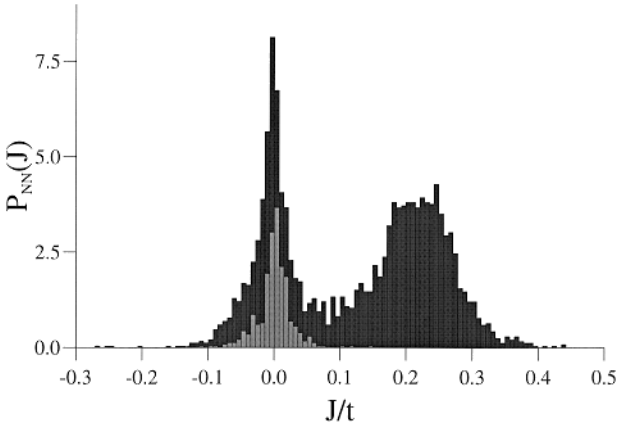

Figure 6. Probability distribution of nearest-neighbour exchange couplings for $(\Delta/t, U/t) = (3, 6)$. Lighter shading denotes the probability distribution of frustrated couplings, as defined in the text.

backbone of the structure. Table 1 shows the percentage of frustrated NN, 2NN and 3NN bonds as a function of interaction strength for $\Delta/t = 3$; 2NN and 3NN couplings are more prone to frustration as one expects. As the interaction strength is decreased, and the effect of disorder correspondingly increases, the degree of frustration increases at all levels, consistent with an ultimate transition [8, 9] to a mean-field spin-glass-like (SG) phase as interaction strength is further decreased.

Although frustrated bonds do occur, note that the Ising-like mean-field states of the effective Heisenberg model are indeed stable for all cases considered above. This is indicated by the facts that (i) for all sites i, $\bar{S}_{iz} h_i^{\mathrm{W}} \leqslant 0$, with the local Weiss field given by $h_i^{\mathrm{W}} = \sum_j J_{ij} \bar{S}_{jz}$ where the sum is over *all* sites j and $\bar{S}_{jz} = \mu_j/|\mu_j| = \pm 1$; and (ii) the static susceptibility matrix of the effective H_{Heis}, equation (2), contains no negative eigenvalues. This is correctly consistent with the fact that the corresponding mean-field UHF states of the Hubbard model are true minima on the Hartree–Fock surface, and are stable against collective particle–hole excitations [8].

To conclude this section, we examine the local sublattice magnetization reduction at one-loop level. This is readily obtained via solution of the LSW equations for the effective Heisenberg Hamiltonian in a site representation (see e.g. references [1, 11]). For the pure Hubbard model, this was calculated in reference [1]. In the strong-coupling limit, the LSW result [11] of a $\sim$15% reduction in the local moment magnitude was correctly recovered. The magnitude of the reduction decreases as the interaction strength is lowered, and the Néel state appears stable against zero-point spin fluctuations throughout the U/t range.

In the presence of significant disorder, however, it is not *a priori* evident that the above situation persists. As discussed in reference [3], disorder 'softens' the RPA collective excitations, leading to a greater density of transverse spin excitations at low frequencies. We anticipate, therefore, that the contribution of such excitations to the magnetization reduction will be enhanced, and one may ask whether this 'softening' is sufficient to destroy the long-ranged order of the mean-field ground state. Further, in the presence of disorder, the magnetization reduction will of course be strongly site differential, dependent on the distribution of spin waves of different energies over sites.

In fact, throughout the AF phase we find that quantum fluctuations are never strong

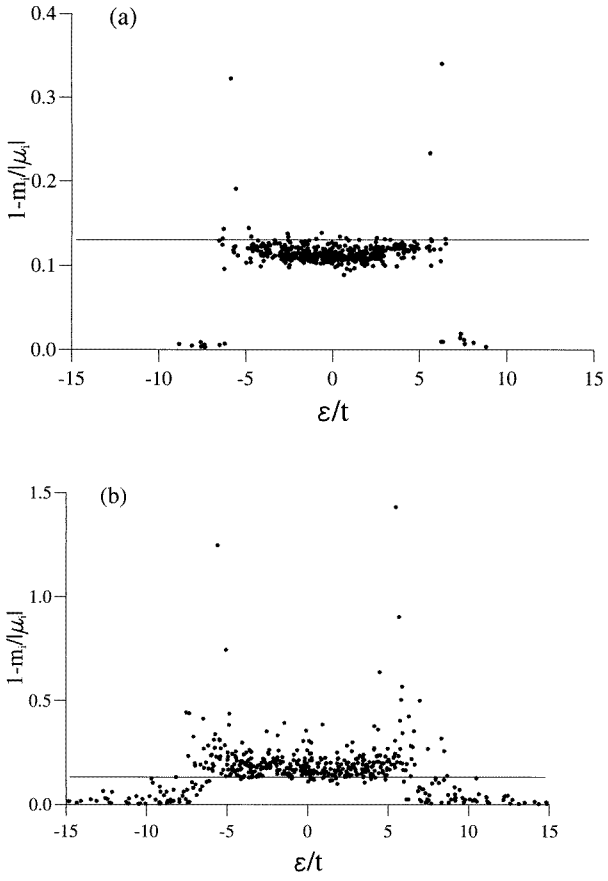

Figure 7. Site-energy resolution of the magnetization reduction as defined in text, for $U/t = 12$ and $\Delta/t = 3$ (a) and 6 (b). The corresponding $\Delta/t = 0$ magnetization reduction is denoted by a horizontal line.

enough to destroy the underlying magnetic order. Figure 7 illustrates the site-differential character of the magnetization reduction. It shows $(|\mu_i| - m_i)/|\mu_i|$ (with m_i the site magnetization at one-loop level) as a function of the site energies ϵ_i, for typical disorder realizations at $U/t = 12$ and $\Delta/t = 3$ (figure 7(a)) and 6 (figure 7(b)). In each case, the strong local moments which occur on sites well within the range $|\epsilon| \lesssim U/2$, and whose magnitudes are close to the non-disordered value, are found to experience a one-loop reduction similar to that at $\Delta = 0$, indicated by a horizontal line. Sites outside these limits, which carry very small moments, have magnetization reductions approaching zero. But a small fraction of sites close to the local moment boundaries ($|\epsilon| \simeq U/2$) have significant magnetization reductions. For $\Delta/t = 3$ (figure 7(a)) these may be up to ~ 3 times the non-disordered value, although none of the moments is completely quenched. On increasing disorder to $\Delta/t = 6$ (figure 7(b)), however, some moment-boundary sites have magnetization reductions in excess of unity, indicating that zero-point fluctuations are sufficient to destroy their local moments. The bulk of the antiferromagnet is nonetheless intact, implying that even at relatively large disorder strengths the local moment description remains a good one.

The site-differential nature of the magnetization reduction can be rationalized microscopically in terms of the effect of disorder on the distribution and localization properties of low-frequency collective excitations, discussed in detail in reference [3]. Figure 9 of reference [3] shows the site resolution of localized and delocalized low-frequency excitations. Strong moments, which occur on sites with bare site energies $|\epsilon_i| \sim 0$, are seen to contribute principally to delocalized excitations, which are essentially the remnants of the $\boldsymbol{q}$-resolvable spin waves of the $\Delta/t = 0$ pure Hubbard model; these sites thus have magnetization reductions similar to the $\Delta = 0$ value, as found above. Localized, low-frequency excitations by contrast predominantly overlap sites at the local moment boundaries—i.e. those in rare environments [8]—typically extending over only one or two sites. It is these sites that experience the strong magnetization reductions which, with increasing disorder, ultimately quench the moments; and that the quenching is local is why the bulk of the AF, and in particular AFLRO, can remain intact.

4. Finite-temperature magnetism

Given the mapping onto an effective spin Hamiltonian, we now focus on the high-temperature paramagnetic phase and consider the transition, as temperature T is lowered, to the magnetically ordered phase. For the pure Hubbard model for $d = 3$, a simple Onsager reaction-field (ORF) approach to the effective Heisenberg model [1, 2] has been found to yield a Néel temperature T_{N} which interpolates successfully between weak and strong coupling, yielding a high-U/t asymptote within 3% of the accepted value from high-temperature series expansions [12], as well as very good agreement with QMC results for spin-correlation functions and static magnetic susceptibilities. In addition, this simple approximation, which provides a self-consistent modification of conventional molecular-field theory (MF) to include the effects of local spin correlations above the ordering temperature, has been found to describe well the paramagnetic phase of the $d = 2$ Heisenberg model [13], and the effect of dimensionality on T_{N} and related quantities in the $d = 2 \rightarrow 3$ anisotropic Heisenberg model [14].

The fundamental thermal excitations of the pure Hubbard model fall into two sets [1, 2]: the low-frequency transverse spin excitations, captured by the effective Heisenberg model equation (2), which in essence describe orientational fluctuations of the local moments, occur on an energy scale set by the effective exchange couplings $\{J_{ij}\}$ and determine the Néel temperature T_{N}; and high-energy Stoner-like thermal excitations which describe longitudinal fluctuations in the local moment magnitudes and have energies of the order of the single-particle band gap (of magnitude $\frac{1}{2}U|\mu|$ and non-zero for all $U/t > 0$). At the level of UHF alone, the latter destroy the local moments at a temperature T_{HF}, obtained by solving the finite-temperature gap equation (equation (5.1) of reference [1]), which is found to go asymptotically as $\frac{1}{4}U$, an asymptote reached in practice for $U/t \gtrsim 4$ [1].

The important point is that this separation of energy scales, which persists [1, 2] over a very wide range of interaction strengths down to weak coupling, $U/t \sim 2$–3, translates thermally into an appreciable temperature range above the Néel temperature T_{N} ($\ll T_{\mathrm{HF}}$) over which physical properties are dominated by the low-lying transverse spin excitations captured by H_{Heis}. The first effects of the Stoner processes on the local moment magnitudes may nonetheless be simply included [1, 2] by replacing the zero-temperature $|\mu_i|$s entering equation (3) for the effective exchange couplings by their self-consistent finite-T values. For $\Delta = 0$, this has a negligible effect on the Néel temperature for moderate to large U/t (although it is necessary for a sensible description of the small-U/t limit).

With disorder present, and throughout the major portion of the disordered AF phase we

consider, the separation of energy scales described above remains largely intact as shown in reference [5], evident e.g. from the persistence of a prominent spin-wave-like band in the full RPA spectrum. We thus proceed in the same way as for the pure Hubbard model, including likewise the T-dependence of the UHF moments μ_i in the effective exchange couplings (equation (3)), obtained via finite-T UHF [15, 16] on which some brief comments are first made.

For the disordered phase of the AHM, as well as for the pure HM, extensive numerical work [17] has shown that the finite-T UHF equations admit only a single low-temperature Ising-like solution. Below T_{HF} the local moments remain collinear, with their ground-state orientations; only their magnitudes vary with temperature, and while these are naturally site differential with disorder present, all moments are found to vanish simultaneously at T_{HF}. And $T_{\mathrm{HF}}(U, \Delta)$ is found to be largely insensitive to disorder strength or the particular disorder realization: a reduction of no more than 10% over $T_{\mathrm{HF}}(U, 0)$ is found at the largest disorder strengths studied.

4.1. Onsager reaction-field theory

The simplest starting point for a finite-temperature theory of the effective Heisenberg model is familiar molecular-field (MF) theory. It proves notationally convenient to rewrite the Hamiltonian as

$$H = -\tfrac{1}{2}\sum_{i\neq j} J'_{ij}\boldsymbol{S}_i \cdot \boldsymbol{S}_j \tag{6}$$

with the trivial sign change $J'_{ij} = -J_{ij}$ (and the $\{J_{ij}\}$ given by equation (3)). The molecular-field susceptibility is then given by

$$\boldsymbol{\chi}^{\mathrm{MF}} = \boldsymbol{\chi}^0[\mathbf{I} - \boldsymbol{\chi}^0\mathbf{J}']^{-1} \tag{7}$$

where $\chi^0_{ij} = C/T\delta_{ij}$ is the Curie susceptibility matrix ($C = S(S+1)/3$ with $S = \frac{1}{2}$). The molecular-field Néel temperature is the temperature at which $\boldsymbol{\chi}^{\mathrm{MF}}$ first diverges on approach from the high-temperature limit, i.e. $T_{\mathrm{N}}^{\mathrm{MF}} = C J_{\max}$ where $J_{\max}$ is the largest eigenvalue of $\mathbf{J}'$. In the pure Hubbard model, $\boldsymbol{\chi}^{\mathrm{MF}}$ is $\boldsymbol{q}$-resolvable; the first divergence in $\chi^{\mathrm{MF}}(\boldsymbol{q})$ occurs at $\boldsymbol{q} = \boldsymbol{\pi}$, indicating that the transition is to a perfectly ordered antiferromagnetic phase. In the presence of disorder, the site resolution or $\boldsymbol{q}$-resolution of the eigenvector corresponding to $J_{\max}$ yields information concerning the nature of the incipient magnetic ordering, the sites on which moments first form and their initial rate of growth (discussed in section 4.3).

The principal, acute failure of molecular-field theory is of course its inability to describe the effects of short-range ordering above the temperature at which long-ranged order sets in. This is alleviated by an ORF treatment, the basic idea of which [18] is that the correct local field to which the spin responds is the field in the absence of the spin in question—the *cavity* field—rather than the molecular (Weiss) field. The cavity field is obtained by subtracting from the molecular field the reaction field, $\boldsymbol{h}_i^{\mathrm{RF}}$, given by $\boldsymbol{h}_i^{\mathrm{RF}} = -\langle \boldsymbol{S}_i\rangle\lambda_i(T)$ where

$$\lambda_i(T) = \sum_j \frac{\langle \boldsymbol{S}_i \cdot \boldsymbol{S}_j\rangle}{S(S+1)} J'_{ij}. \tag{8}$$

The ORF susceptibility matrix, obtained in direct analogy to molecular-field theory but with a spin responding to its cavity field, is then given by

$$\boldsymbol{\chi} = \boldsymbol{\chi}^0[\mathbf{I} - \boldsymbol{\chi}^0(\mathbf{J}' - \boldsymbol{\lambda})]^{-1} \tag{9}$$

where the local reaction-field matrix $[\boldsymbol{\lambda}]_{ij} = \lambda_i(T)\delta_{ij}$. To determine the latter self-consistently we enforce the fluctuation-dissipation theorem in its high-temperature form:

$\langle \boldsymbol{S}_i \cdot \boldsymbol{S}_j \rangle = 3T\chi_{ij}$ and, in particular, $\chi_{ii} = C/T$ for *each* site i. Equation (8) thus becomes a coupled set of N self-consistency equations for the $\lambda_i(T)$, namely

$$\lambda_i(T) = \sum_j ([\mathbf{I} - \boldsymbol{\chi}^0(\mathbf{J}' - \boldsymbol{\lambda})]^{-1})_{ij} J'_{ij}. \tag{10}$$

The susceptibility matrix then follows directly; and from equation (9) the ORF transition temperature is that for which the largest eigenvalue of $\mathbf{J}' - \boldsymbol{\lambda}$ becomes equal to T/C, with the corresponding eigenvector describing the nature of incipient ordering at the transition.

Before presenting the results of the above treatment, we comment on the connection between the ORF approach and the spherical approximation. In the non-disordered limit, and within the high-T paramagnetic phase, the ORF is equivalent to the mean-spherical approximation [19, 20] (MSA). This is not so in the presence of disorder. The mean-spherical constraint $N^{-1}\sum_i \langle \boldsymbol{S}_i^2 \rangle = C$ is in fact equivalent to enforcing the fluctuation-dissipation theorem *only on average*. This is incorrect for the present system: a clear symptom is that, in the high-temperature limit, while the mean local susceptibility $\langle \chi \rangle = N^{-1}\sum_i \chi_{ii}$ is given by the Curie law, individual sites may have susceptibilities considerably in excess of the free-spin value—an obviously unphysical result. Further, it fails to capture any inhomogeneity in the local reaction field, which is important in describing the ordering transition at moderate to large disorder, as discussed in the following sections. The two approximations become equivalent for a disordered system only in the limit of infinite-ranged interactions (such as the Sherrington–Kirkpatrick model for a spin glass [21]) where local inhomogeneities are eliminated.

Finally we note that, for an arbitrary disordered Heisenberg model, the correct functional-integral analogue of ORF is the saddle point approximation obtained by taking the limit of infinite spin dimensions [22]. This approach may be shown to yield results for the paramagnetic phase identical to those of ORF discussed in the present work.

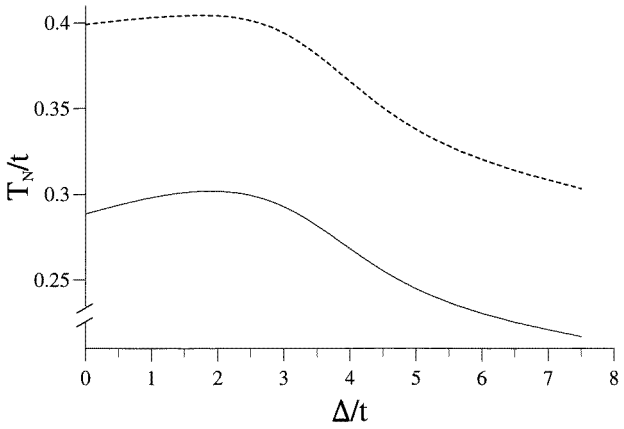

Figure 8. ORF Néel temperature T_N of the AHM for $U/t = 12$ as a function of the disorder strength (solid line); the MF temperature T_N^{MF} is shown for comparison (dashed line).

4.2. Thermal phase diagram of the AHM

Figure 8 shows the effect of disorder on the ORF Néel temperature T_N for fixed interaction strength $U/t = 12$; the molecular-field T_N^{MF} is shown for comparison. The T_N shown is an

average over many disorder realizations at any Δ/t point, and we add that little variation in the ordering temperature is found from realization to realization. Both T_N and T_N^{MF} show the same trend with increasing disorder: a slight initial increase, consistent with the disorder-induced strengthening of the exchange couplings (see section 3 and figure 5), followed by a steady decline as the exchange couplings correspondingly decrease. Note that the ORF Néel temperature is always considerably lower than T_N^{MF}, indicating that short-ranged ordering above the Néel temperature is significant at all disorder strengths.

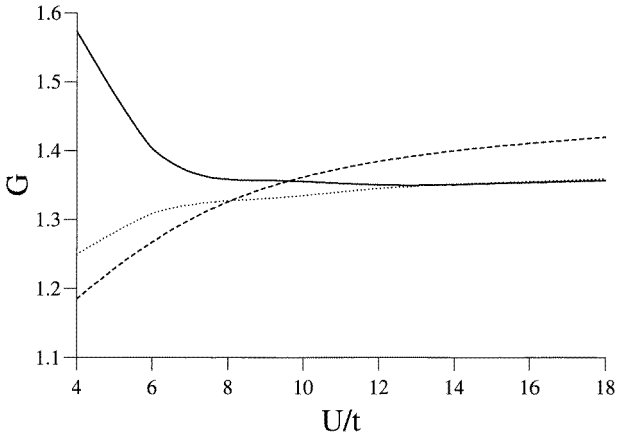

Figure 9. The ratio $G = T_N^{MF}/T_N$ as a function of interaction strength for $\Delta/t = 3$ (solid line). Also shown is the $\Delta/t = 0$ result (dotted), and G obtained via the MSA (dashed line).

An interesting aspect of the role of disorder is the increasing importance of short-range order effects as U/t is lowered. This is illustrated by considering the ratio of the molecular-field Néel temperature T_N^{MF} to the ORF Néel temperature T_N: $G = T_N^{MF}/T_N$. The greater the degree of short-ranged order sustainable above T_N, the lower the temperature at which long-ranged order sets in, and the higher the value of G. Figure 9 shows the variation of G with U/t for $\Delta/t = 3$, together with the $\Delta/t = 0$ result for comparison. As $U/t \to \infty$, both curves tend towards the limit $G = 1.516$ for the non-disordered NN AF Heisenberg model [13].

As U/t is reduced from the strong-coupling limit, G for the pure Hubbard model decreases steadily, consistent with the increasing range of effective spin interactions [1, 2] and the consequent improvement in accuracy of molecular-field theory. With disorder present, however, very different behaviour is observed: G actually *increases* rapidly with decreasing U/t below $\sim$6, showing the increasing importance of local spin fluctuations as U/t is decreased towards the value ($U/t \simeq 3$) at which, for $T = 0$, the UHF mean-field ground state becomes a SG. This concurs with an argument given by Cyrot [23] that inclusion of reaction-field effects in a spin-glass phase is crucial (and indeed the celebrated TAP equations [24] for a classical spin glass amount to an approximate inclusion of such effects [25, 26]). Finally, figure 9 also shows G obtained for $\Delta/t = 3$ via the MSA, the behaviour of which is qualitatively akin to that in the absence of disorder; this illustrates further the deficiencies of the MSA with disorder present, as discussed above.

Figure 8 also illustrates a somewhat counterintuitive effect of disorder on T_N: for sufficiently large U/t, increasing disorder initially *raises* the Néel temperature, at both MF and ORF levels. This effect was also observed by Ulmke *et al* [10] in quantum Monte Carlo

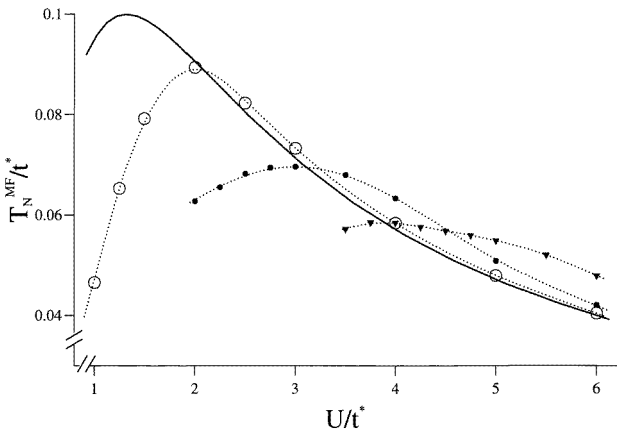

Figure 10. MF Néel temperature T_N^{MF}/t_* as a function of U/t_* with $t_* = 2\sqrt{6}t$, for the $d = 3$ simple cubic lattice with semi-elliptic site disorder of full width Δ. For fixed disorder $\Delta/t_* = 0$ (solid line), 2 (open circles), 4 (solid circles) and 6 (triangles).

(QMC) studies of an infinite-dimensional Anderson–Hubbard model on a Bethe lattice, with both semi-elliptic and binary-alloy-type site-disorder distributions: figure 4(b) of reference [10] shows the Néel temperature as a function of U/t_* where $t = t_*/2\sqrt{z}$ (with coordination number $z \to \infty$), for uncorrelated semi-elliptic disorder of (full) width $\Delta/t_* = 0, 2, 4, 6$; the enhancement of the Néel temperature by disorder is particularly evident in the difference between the $\Delta/t_* = 2$ and $\Delta/t_* = 4$ curves. To compare the present theory with the $d = \infty$ QMC results, we have repeated our $d = 3$ calculations for semi-elliptic site-disorder distributions; and we consider explicitly T_N^{MF}, since ORF corrections vanish in the large-d limit and molecular-field theory becomes exact for strong coupling [13]. Figure 10 shows the resultant T_N^{MF}, scaled by the appropriate $t_* = 2\sqrt{6}t$, as a function of U/t_* for a semi-elliptic distribution of site energies of width $\Delta/t_* = 0, 2, 4, 6$. (Since our theory is inapplicable in the spin-glass regime, results are shown only for values of U/t_* yielding an antiferromagnetic ordered phase.)

Clearly, the trends observed for $d = \infty$ are also observed for the present system. In particular, for sufficiently large U/t_*, T_N^{MF} is enhanced by initially increasing disorder. This is seen directly in figure 8, and reflects the disorder-induced enhancement of effective exchange couplings illustrated in figure 5 (and discussed above); the microscopic origins of the latter have been given in reference [10]. One quantitative difference between figure 10 and the results of reference [10] is worth noting: for large U/t_*, $T_N^{d=\infty} > T_N^{MF}(d = 3)$, since the effects of low-energy spin waves, which act to reduce the effective exchange couplings and hence the Néel temperature from its 'Ising' value, are entirely absent for $d = \infty$ [27]. Although the strong qualitative similarity between figure 10 and figure 4 of reference [10] is very encouraging, we remind the reader that the 'correct' ordering temperature for the finite-d system is the ORF T_N, which is reduced from its molecular-field counterpart by reaction-field effects, analogously to the behaviour shown in figure 8.

4.3. Nature of the paramagnetic–antiferromagnetic transition

While the ORF theory discussed in section 4.1 applies only to the paramagnetic regime, it can give insight into the nature of the state into which the system condenses: at the

Néel temperature, the spatial distribution of the eigenvector corresponding to the divergent eigenvalue of $\boldsymbol{\chi}$, equation (9), yields information on which sites first obtain moments, their relative phases and initial rate of growth. The eigenvectors $\boldsymbol{\Phi}_\alpha$ of $\boldsymbol{\chi}$ are defined via $\sum_j \chi_{ij}\Phi_{j\alpha} = \gamma_\alpha \Phi_{i\alpha}$ (with γ_α the associated eigenvalue), and the $\{\Phi_{j\alpha}\}$ describe the spatial distribution over sites of the eigenvector. At molecular-field level, the eigenvectors of $\boldsymbol{\chi}^{\mathrm{MF}}$ (equation (7)) are solely those of the exchange-coupling matrix $\mathbf{J}'$; while at ORF level by contrast the diagonal elements $\{\lambda_i(T)\}$ (see equation (10)) are in addition self-consistently determined for each site, and vary strongly with T as the Néel temperature T_{N} is approached.

For the pure Hubbard model, the Fourier-resolved susceptibility $\chi(\boldsymbol{q})$ first diverges at $\boldsymbol{q} = \boldsymbol{\pi}$ for all U/t, implying that the low-temperature phase has AFLRO. In a disordered system, we anticipate the possibility of contributions to the divergent eigenmode from many $\boldsymbol{q}$-vectors. This raises the possibility that, for sufficiently strong disorder, the eigenvector may be localized in the Anderson sense [28, 29]. The eigenvalue spectrum of $\boldsymbol{\chi}$ is formally equivalent to that of a tight-binding model with correlated diagonal and off-diagonal disorder. Following conventional arguments (see e.g. reference [30]), states at the band edges of the spectrum tend to be the first to localize, with states near the centre remaining extended up to larger values of the disorder. (Note that this scenario could not arise in an effective spin model with infinite-ranged interactions, such as the SK model, where all eigenvectors of $\boldsymbol{\chi}$ are inevitably extended [25], or in infinite dimensions.) For short-ranged models, a predicted condensation via a localized mode cannot represent a true phase transition. Hertz *et al* [29] have argued that the true transition temperature and corresponding magnetic ordering are in this case given by the first extended eigenstate (i.e. the state at the upper mobility edge) in the spectrum of $\boldsymbol{\chi}$.

Our first interest is to assess whether the Néel temperature, shown in figure 8, corresponds to a genuine phase transition. Finite-size calculations cannot of course yield definitive information on localization, but are we believe sufficient to permit qualitative conclusions to be drawn. The inverse participation ratio [31] (IPR) defined by $L_\alpha = \sum_i \Phi_{i\alpha}^4$ for any eigenmode α, is a convenient means of distinguishing localized from extended eigenvectors. $L_\alpha = 1$ for an atomically localized eigenvector, while for an infinite system $L_\alpha = 0$ for an extended state. In a finite-size system, where $L > 0$ necessarily, a size-dependent IPR threshold separating localized and extended modes ought in principle to be established by finite-size scaling. In the present problem this is computationally prohibitive, and we adopt a threshold of $L \sim 0.05$–0.1 (as appropriate to a disordered tight-binding model at the chosen system size of $N = 216$ [32]). This should not itself be taken very seriously: its purpose here is purely qualitative.

For $U/t = 12$ (appropriate to figure 8 for T_{N}), and for all values of Δ/t studied (up to $\Delta/t = 7.5$), the divergent eigenvector in both the MF and ORF treatments is in fact found to be clearly extended, with an IPR well below the above threshold. This leads us to believe that the condensation at T_{N} indeed represents a genuine phase transition to a state with magnetic LRO. It is further supported by $\boldsymbol{q}$-resolution of the divergent eigenvectors: although increasingly 'dirtied' by disorder, these are strongly peaked at $\boldsymbol{q} = \boldsymbol{\pi}$, with little weight at other $\boldsymbol{q}$-vectors. The thermal transition is thus to a disordered AF phase, and the above results concur well with the behaviour of the $T = 0$ UHF local moment structure factor $\mu(\boldsymbol{q})$, discussed in section 2.

Finally, for $U/t = 12$ and $\Delta/t = 7.5$, figure 11 shows the site-energy resolution of the ordering vector $\boldsymbol{\Phi}_m$, given by $|\Phi(\epsilon)| = N_\epsilon^{-1} \sum_{i:\epsilon_i=\epsilon} |\Phi_{im}|^2$ (with N_ϵ the number of sites of given site energy ϵ). This has greatest weight on those sites with $|\epsilon| \lesssim U/2$ which, at $T = 0$, carry large UHF local moments; and that the initial rate of condensation is greatest for such sites is implied by the distribution of exchange couplings described in section 3: it is these

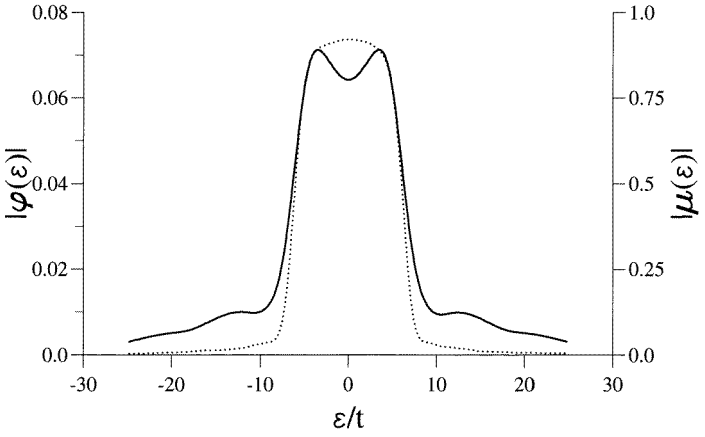

Figure 11. Site-energy resolution of the eigenvector corresponding to the divergent eigenvalue of χ, $|\phi(\epsilon)|$ (solid, left-hand scale); and the corresponding $T = 0$ UHF local moment profile $|\mu(\epsilon)|$ (dotted, right-hand scale) for $(\Delta/t, U/t) = (7.5, 12)$.

sites that have the largest local J_{ij}s and hence the strongest internal, ordering fields. In fact, the $|\Phi(\epsilon)|$ is in striking accord with the local moment profile $|\mu(\epsilon)| = N_\epsilon^{-1} \sum_{i:\epsilon_i=\epsilon} |\mu_i|$ for the $T = 0$ UHF moments, also shown in figure 11.

In summary, we have investigated the disordered antiferromagnetic phase of the Anderson–Hubbard model via a mapping, at $T = 0$, of its low-energy transverse spin excitations onto those of a self-consistent underlying Heisenberg model. Taking it in conjunction with a simple Onsager reaction-field approach to the thermal paramagnetic phase, we have used the mapping to study the Néel temperature as a function of disorder and interaction strengths, and the nature of the ordering transition. The mapping may also in principle be used to investigate thermal properties of the low-temperature magnetically ordered state, although extension of the ORF approach to ordered phases has yet to be obtained, even for the classical Ising model; we are currently working on this problem.

Acknowledgments

We would like to thank the EPSRC and the Royal Commission for the Exhibition of 1851 for financial support.

References

[1] Tusch M A, Szczech Y H and Logan D E 1996 *Phys. Rev.* B **53** 5505
[2] Szczech Y H, Tusch M A and Logan D E 1995 *Phys. Rev. Lett.* **74** 2804
[3] Szczech Y H, Tusch M A and Logan D E 1997 *J. Phys.: Condens. Matter* **9** 9621
[4] Singh A and Tešanović Z 1990 *Phys. Rev.* B **41** 614
[5] Schrieffer J R, Wen Z-G and Zhang S-C 1989 *Phys. Rev.* B **39** 11 663
[6] Moriya T 1985 *Spin Fluctuations in Itinerant Electron Magnetism* (Berlin: Springer)
[7] Strictly speaking, this is correct for bounded site-energy distributions; but it holds in practice for the Gaussian site-disordered model considered here.
[8] Tusch M A and Logan D E 1994 *Phys. Rev.* B **48** 14 843
[9] Rowan D G, Szczech Y H and Logan D E 1995 *J. Phys.: Condens. Matter* **7** 6853
[10] Ulmke M, Janiš V and Vollhardt D 1995 *Phys. Rev.* B **51** 10 411

[11] Manousakis E 1991 *Rev. Mod. Phys.* **63** 1
[12] Rushbrooke G S, Baker G A and Wood P J 1974 *Phase Transitions and Critical Phenomena* vol 3, ed C Domb and M S Green (New York: Academic) ch 5
[13] Logan D E, Szczech Y H and Tusch M A 1995 *Europhys. Lett.* **30** 307
[14] Eastwood M P and Logan D E 1995 *Phys. Rev.* B **52** 9455
[15] See, e.g.,
de Gennes P-G 1966 *Superconductivity of Metals and Alloys* (New York: Benjamin)
Brack M and Quentin P 1974 *Phys. Lett.* **52B** 159
[16] Brandow B H 1977 *Adv. Phys.* **26** 651
[17] Szczech Y H 1996 *DPhil Thesis* Oxford University
[18] Onsager L 1936 *J. Am. Chem. Soc.* **58** 1486
[19] Berlin T H and Kac M 1952 *Phys. Rev.* **86** 821
[20] Brout R and Thomas H 1967 *Physics* vol 3 (Long Island City, NY: Physics Publishing) p 317
[21] Sherrington D and Kirkpatrick S 1975 *Phys. Rev. Lett.* **35** 1972
[22] Stanley H E 1968 *Phys. Rev.* **176** 718
[23] Cyrot M 1979 *Phys. Rev. Lett.* **43** 173
[24] Thouless D J, Anderson P W and Palmer R G 1977 *Phil. Mag.* **35** 593
[25] Binder K and Young A P 1986 *Rev. Mod. Phys.* **58** 801
[26] Chowdhury D and Mookerjee A 1984 *Phys. Rep.* **114** 1
[27] Logan D E, Eastwood M P and Tusch M A 1996 *Phys. Rev. Lett.* **76** 4785
Logan D E, Eastwood M P and Tusch M A 1997 *J. Phys.: Condens. Matter* **9** 4211
[28] Anderson P W 1970 *Mater. Res. Bull.* **5** 594
[29] Hertz J A, Fleischman L and Anderson P W 1979 *Phys. Rev. Lett.* **43** 942
[30] Mott N F 1990 *Metal–Insulator Transitions* (London: Taylor & Francis)
[31] Bell R J and Dean P 1970 *Discuss. Faraday Soc.* **50** 55
[32] Chang T M, Bauer J D and Skinner J L 1990 *J. Chem. Phys.* **93** 8973